Adsorption-induced deformation of microporous materials: coal swelling induced by CO2-CH4 competitive adsorption

Laurent Brochard, Matthieu Vandamme, Roland J. M. Pellenq, Teddy Fen-Chong

Adsorption-induced deformation of microporous materials: coal swelling induced by CO_2-CH_4 competitive adsorption

Laurent Brochard,[†] Matthieu Vandamme,[†] Roland J.-M. Pellenq,[*,‡] and Teddy Fen-Chong[†]

Université Paris-Est, Laboratoire Navier (ENPC/IFSTTAR/CNRS), Ecole des Ponts ParisTech, 6 & 8 avenue Blaise Pascal, 77455 Marne-la-Vallée, France., and CINaM-CNRS, Campus de Luminy, 13288 Marseille cedex 09, France, and CEE-MIT, 77 Massachusetts avenue, 02139, Cambridge, MA, USA.

E-mail: pellenq@cinam.univ-mrs.fr

Abstract

Carbon dioxide injection in coal seams is known to improve the methane production of the coal seam, while ensuring a safe and long term carbon sequestration. This improvement is due to the preferential adsorption of CO_2 in coal with respect to CH_4: an injection of CO_2 thus results in a desorption of CH_4. But this preferential adsorption is also known to cause a differential swelling of coal, which results in a significant decrease in the reservoir permeability during the injection process. Recent studies have shown that adsorption in coal micropores (few-angström large) is the main cause of the swelling. In this work we focus on the competitive adsorption behavior of CO_2 and CH_4 in micropores. We perform molecular simulations

[†]Université Paris-Est
[‡]CNRS and MIT

of adsorption with a realistic atomistic model for coal. The competitive adsorption is studied at various temperatures and pressures representative of those in geological reservoirs. With the help of a poromechanical model, we then quantify the subsequent differential swelling induced by the computed adsorption behaviors. The differential swelling is almost insensitive to the geological temperatures and pressures here considered and is proportional to the CO_2 mole fraction in the coal.

Introduction

Coal Bed Methane production from unminable coal seams is an important source of natural gas: In 2008 it amounted to 10% of the total natural gas production in the United States. Large commercial projects also operate in Australia, China and India.[1] Most of the gas is stored in the coal material under adsorbed form in micropores which are a few angström or a few nanometer large. Gas extraction proceeds by desorption from the coal material and by convective transport through a set of small natural fractures (cleats), which are typically spaced by a few centimeters. Most of the permeability of the coal reservoir comes from the cleat network, but the permeability of those cleats strongly depends on the underground stress.[2–4] The adsorption affinity of carbon dioxide in coal is higher than that of methane. Therefore, an injection of CO_2 in coal beds improves the recovery of CH_4: in the case of the Allison unit[5] 95% of all the methane could be recovered after an injection of CO_2, compared to only 77% with no injection of CO_2. Moreover, this technique enables to store CO_2, thus lowering the CO_2 emissions associated with consumption of such natural gas.[6,7] This process is known as 'enhanced coal bed methane recovery' (ECBM).

A major problem encountered in the current and past ECBM demonstrators is an important loss of permeability of the reservoir consecutive to the desorption of CH_4 and to the adsorption of CO_2. In the case of the Allison unit,[5] permeability decreased by about one order of magnitude near the injection wells. This loss of permeability is attributed to the so-called 'differential swelling' phenomenon: a coal sample swells more in a CO_2 atmosphere than in a CH_4 atmosphere at the same pressure.[3,8,9] This swelling leads to a closure of the cleat network which results in a decrease

of the permeability of the reservoir.[2,10] Coal swelling is known to be due to adsorption. A proper understanding of the adsorption behavior of CO_2 and CH_4 and of the impact of adsorption on the mechanical behavior of coal is of great interest in field applications in order to design wells completion and plan mitigation methods against coal swelling.

Coal, by nature, is a disordered porous material whose carbon content weight fraction ranges from 60% to 95%. It exhibits a complex pore structure with a typical dual porosity:[11] very small micropores (radius smaller than 1 nm) and larger mesopores (radius greater than 1 nm). Due to the very high adsorption energies of micropores, adsorption behaviors in such pores differs from those in mesopores. Experimental[12] and theoretical[13] studies have shown that the differential swelling of coal is mostly explained by adsorption in micropores.

A lot of laboratory experiments of adsorption and swelling of coal have been performed and many results are available in the literature.[8,9,14–16] Molecular simulation is an investigation tool which interestingly complements laboratory experiments, by making it possible to investigate adsorption in micropores separately from mesopores and to apply any condition to the medium, for instance underground conditions. Our aim in this paper is to study the competitive adsorption of CO_2 and CH_4 in coal micropores with a realistic molecular model for coal. The competitive adsorption is studied under various temperatures and bulk pressures, in order to assess the sensitivity of the differential swelling phenomenon to the depth of the site of injection. Once a quantitative estimate of the adsorbed amounts is obtained, it is then possible to predict the evolution of the differential swelling depending on the CO_2-CH_4 mixture composition. Indeed, the influence of adsorption on the mechanical behavior can be estimated with appropriate models.[13,17–20]

The first part of this paper is dedicated to the implementation of the molecular simulations. The molecular models selected for coal, carbon dioxide and methane, and the mutual interactions models are presented. In a second part, we present and discuss the results of the adsorption simulations of the CO_2-CH_4 mixture in micropores. Using the poromechanical model of Brochard et al.,[19,20] we then give a quantitative estimate of the differential swelling of coal induced by the replacement of methane by carbon dioxide at temperatures and pressures representative of field conditions.

Computational details

In this part, we present the temperatures and pressures considered and the numerical methods employed in this work. Then we describe in details the molecular models we used for coal, methane and carbon dioxide, as well as for their mutual interactions.

Temperature and pressure

In an actual coal bed reservoir in which carbon dioxide is injected, the coal matrix is exposed to a mixture of CO_2 and CH_4 whose composition varies. Indeed, during the injection process, CO_2 gradually replaces CH_4. In a first approximation, we will consider that, during this process, the temperature and the fluid pressure remain constant and equal to the geothermal temperature and to the hydrostatic pressure, respectively. Such a description is approximative: the temperature may vary with the heat transported by the injected fluid and the fluid is actually injected at a pressure higher than the pressure that prevails in the reservoir.

We selected five sets of temperature and pressure conditions that correspond to the following injection site depths: 300 m, 600 m, 900m, 1200 m and 1500m. These depths correspond to the range of injection site depths considered for carbon dioxide sequestration.[7] The corresponding temperatures and pressures were obtained by considering an average geothermal gradient of $25^\circ\mathrm{C/km}$, a surface temperature of 15°C, a hydrostatic pressure gradient and a surface pressure of 101325 Pa. For the pressure gradient, we considered a water density $\rho_{H_2O} = 1000\ \mathrm{kg/m^3}$ and a gravitational acceleration of $g = 9.81\ \mathrm{m/s^2}$. The temperatures and pressures considered ranged from 295.7 K and 3.04 MPa for the shallowest site (300 m) to 325.7 K and 14.82 MPa for the deepest site (1500 m), respectively, with both parameters increasing linearly with the depth of the site.

Algorithm and boundary conditions

The adsorption simulations are Monte Carlo simulations performed in the Grand Canonical statistical ensemble, in which the chemical potentials of the molecules (μ_{CO_2} for carbon dioxide and μ_{CH_4} for methane), the volume V and the temperature T of the system are imposed.[21–23] We apply periodic boundary conditions and molecules are interacting according to the 'minimum image convention'.

Prior to the grand canonical simulations, a first step is to determine the chemical potentials of the two species in the mixture. At a given temperature and bulk pressure, the chemical potentials of CO_2 and CH_4 in a CO_2-CH_4 mixture can be obtained by simulating the bulk mixture in the isobaric isothermal ensemble. These simulations are Monte Carlo simulations as well (NPT Monte Carlo), in which the number N of molecules, the pressure P and the temperature T of the system are imposed by the external reservoir.[21–23] The chemical potentials are measured with the Widom insertion method.[21] We also apply the periodic boundary conditions and use the minimum image convention.

Molecular model for coal

Coal is a complex mixture of organic and inorganic matter, made of hundreds of elementary constituents.[24] The residues of the coalified plants (called the macerals) are the main constituents of coal and of its organic matter. The remaining matter in coal is mostly inorganic minerals which contribute little to the adsorption of gases.[7,25,26] Accordingly, we focus on the organic matter of coal in this work. Carbon atoms are the main constituent of coal and represent about 80% of the total mass of coal on a dry ash free basis.[27] Apart from carbon, the dry macerals contain mainly oxygen, hydrogen, nitrogen, and sulfur. The contents of oxygen and hydrogen are by far the most significant after the content of carbon, since oxygen and hydrogen each constitute more than 4% of the total mass of coal.[27] The chemical composition, maceral composition, and mineral composition vary widely from one coal to another. Accordingly the swelling of coal upon adsorption varies widely from one coal sample to the other[8,9,14,15] and the specific behavior of each grain of

maceral makes coal swell in a heterogeneous manner.[28]

In this work, we study the adsorption of methane and carbon dioxide by molecular simulation on a realistic molecular structure of coal. This study is based on one specific structure of coal and thus does not account for the variability of natural coal. Accordingly our results are not fully representative of the complexity of natural coal. This work aims at providing a first hint at the adsorption and adsorption-induced swelling in coal.

Coals are glassy, strained, cross-linked macromolecular systems[29] and exhibit an amorphous molecular structure with aromatic skeleton of various sizes stacked in a few layers.[30] Different molecular models for porous carbons have been developed, which can be classified into three main categories according to their complexity:

- The slit pore model is a simple molecular model for graphite-like materials.[31] The model is based on an analytic formulation of the solid-gas energy of interaction, the 'Steele $10-4-3$ potential', which assumes that the solid matrix is only composed of carbon atoms distributed in graphene layers. The implementation of this model is simple and its computational cost is low. Therefore, this model has been widely used to simulate physical adsorption of gases in porous carbons.[17,32–34] However, independent and unconnected graphite-like slit pores are not representative of the amorphous and chemically heterogeneous structure of natural coal.

- Chemically heterogeneous models[35,36] account for the presence of oxygen and hydrogen atoms observed in bituminous and sub-bituminous coal. A model for coal is obtained by modifying graphite surfaces in order to account for topological and chemical heterogeneities. Selected carbon atoms from the top graphene layer are either removed entirely or replaced with oxygen- and hydrogen-containing functional groups, in order to obtain a content in oxygen and hydrogen similar to that observed in natural coal. Physical adsorption is then simulated by using Lennard-Jones and electrostatic interaction potentials.

- Molecular models obtained by reverse Monte Carlo methods[37–41] account for both the structural and chemical heterogeneities in porous carbons. The reverse Monte Carlo methodology

is a reconstruction technique that consists in creating a molecular structure by fitting simultaneously various experimental results such as X-ray scattering data, coordination number of the carbon atoms, average covalent bond angles and/or total interaction energy. The various fitting parameters are aggregated in a single cost function which is minimized. The models created exhibit amorphous porous structures with aromatics rings of various sizes. These amorphous structures are validated by comparing simulated adsorption in these structures to experimental adsorption data.[40] Those models are consistent with TEM image analysis.[37]

In this work, we used the reverse Monte Carlo models as molecular models for coal: their structural and chemical heterogeneities make them more suitable to reflect the adsorption behavior of natural coal. Among various reverse Monte Carlo models, we used the CS1000 model developed by Jain et al.[39] (see Figure 1). CS1000 is the molecular representation of a high density porous saccharose coke obtained by pyrolyzing pure saccharose at 1000°C in a nitrogen flow. The reconstruction method used is the 'Hybrid Reverse Monte Carlo' (HRMC) method, which aims at minimizing the total energy of interaction while fitting the experimental pair correlation function between the atoms of carbon. The HRMC method ensures that the molecular structure reconstructed is stable and exhibits the main morphological characteristics of the saccharose coke. We chose the CS1000 model of Jain et al.[39] because its characteristics, in terms of density, porosity and composition are close to those of natural coal:

Porosity and pore size distribution: Experimental measurements[11] of the pore size distribution of coal indicate a clear separation between micropores, whose radius is smaller than 10 Å, and mesopores, whose radius is larger than 10 Å. Due to its size ($25 \times 25 \times 25$ Å^3), the CS1000 sample does not contain mesopores. The porosity in the CS1000 model, probed by a hard sphere with a 3 Å diameter, is 14%. This value for the porosity, which accounts for the microporosity only, is in good agreement with experimental values.[11] Micropores in coal vary in size but do not extend above 1 nm. The CS1000 model captures well these features with a wide distribution of micropore sizes[40] and a maximum size of the micropores of 8 Å.

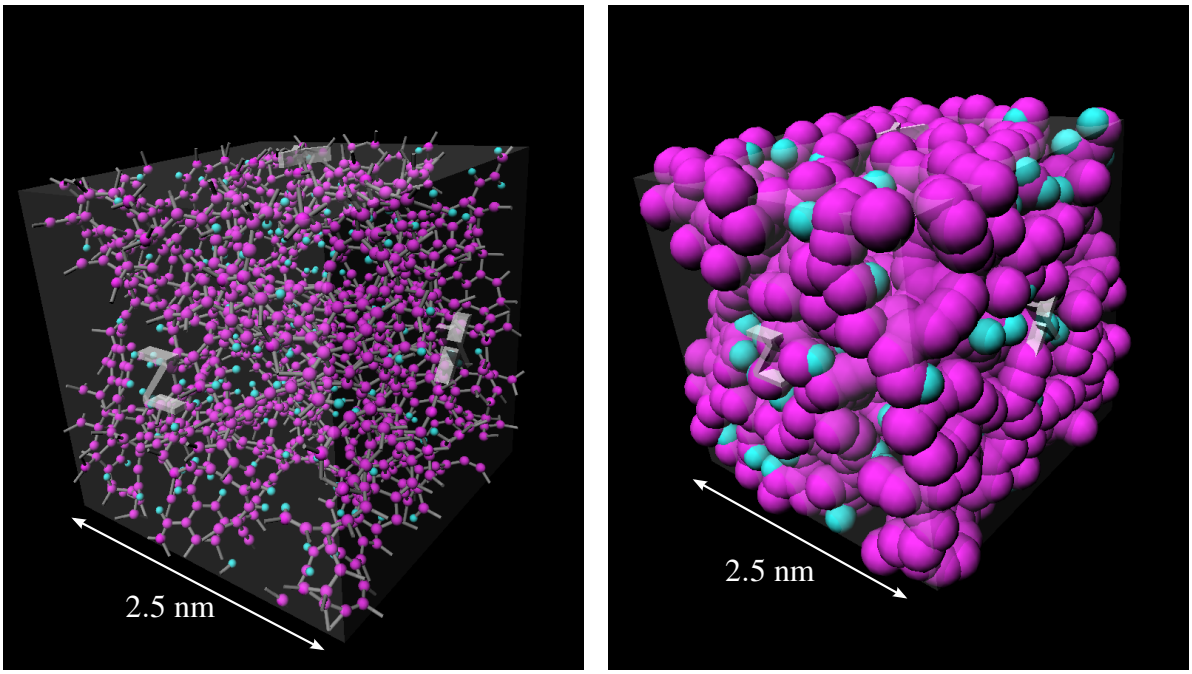

(a) (b)

Figure 1: Representations of the CS1000 molecular model, representative of the nano-structure of coal. Representation of the covalent bonds (a) and representation of the volume occupied by the Van der Waals radii of the atoms (b).

Density: The density of the CS1000 model is 1584 kg/m^3, which is in the high range of helium densities of coal, generally measured between 1250 kg/m^3 and 1600 kg/m^3.[7,11,42]

Chemical heterogeneity: The CS1000 model includes carbon and hydrogen atoms. Oxygen is not accounted for, since oxygen represents less than 1% in mass in the saccharose coke. The proportion of hydrogen atoms in CS1000, which is equal to 1.2% in mass, is lower than the proportion observed in natural coal, which is around 5% in mass. The absence of oxygen atom is an important drawback of the CS1000 model. Indeed, the electronegativity of the atom of oxygen is high compared to that of carbon, which means that the distribution of charge in the coal matrix depends significantly on the presence of oxygen. Therefore, the CS1000 model should not be used to simulate the adsorption of polar fluids in coal, which strongly depends on the distribution of charge in the coal matrix. In this work, we focus on methane and carbone dioxide, which are nonpolar fluids and for the adsorption of which we disregard the effect of the presence of atoms of oxygen in the coal matrix.

In this molecular modeling, we consider the solid to be rigid so that we do not need to compute the interaction energy between the atoms of the solid. This approximation is reasonable since the atomic structure of coal is glassy at the temperatures of interest, i.e., the motions of the atoms of the solid skeleton remain very small. By doing so, the results correspond to an adsorption at zero strain.

Molecular models for the fluids

Methane

Methane was simulated with a Lennard-Jones potential. The interaction energy $U_{CH_4-CH_4}$ between two molecules of methane depends on the distance r between the centers of the molecules:

$$U_{CH_4-CH_4}(r) = 4\varepsilon_{CH_4}\left(\left(\frac{\sigma_{CH_4}}{r}\right)^{12} - \left(\frac{\sigma_{CH_4}}{r}\right)^{6}\right) \quad (1)$$

where σ_{CH_4} and ε_{CH_4} are the Lennard-Jones parameters for methane. We used the Lennard-Jones parameters proposed by Kurniawan et al.,[43] adapted to the simulation of methane in supercritical conditions (pressure up to 20 MPa and temperature greater than 190 K): $\sigma_{CH_4} = 3.751$ Å and $\varepsilon_{CH_4} = 148 \cdot k_B$, where k_B is the Boltzmann constant.

To check the validity of this model for underground conditions, we performed molecular simulations of pure methane in the grand canonical ensemble at a temperature of 310 K and for fugacities ranging from 0 to 10 MPa in a cubic simulation box of size $50 \times 50 \times 50$ Å^3. The fugacity is related to the chemical potential μ by the relation[22] $\mu = k_B T \ln\left(\Lambda^3\right) + k_B T \ln\left(f/\left(k_B T\right)\right)$, where $\Lambda = \sqrt{h^2/\left(2\pi m k_B T\right)}$ is the thermal de Broglie wavelength and h is the Planck constant. For distances between molecules larger than 23 Å, the energy of interaction was set to zero, which is reasonable regarding the value of σ_{CH_4} and consistent with the size of the simulation box. For all these simulations, we computed the average density and the pressure with the virial estimate.[21,44,45] We display in Figure 2 the pressures and densities obtained by molecular simulation and those obtained with an experimental equation of state.[46] The uncertainties of the averages calculated were estimated with the block averaging method.[22] The relative standard deviations of both the pressure and the density were lower than 0.6%. From this comparison, we conclude that the Lennard-Jones model used here enables to capture well the bulk properties of methane in the range of pressures and temperatures of interest for our study.

Carbon dioxide

We used the EPM model developed by Harris and Yung[47] to simulate CO_2. The molecule is represented by three Lennard-Jones centers (one for each atom) and three point charges at the same centers. The molecule is rigid. Harris and Yung developed a modified version of the EPM model in which the angle between the covalent bonds can vary. This modification was introduced because a marginal deviation from the linear geometry is observed experimentally in supercritical conditions. This modified EPM model is more precise than the original EPM model in underground conditions, but its computational cost is higher because an additional degree of freedom has to be

taken into account for each molecule. We decided to use the original EPM model in this work, because we were not interested in introducing much refinement to the molecular model of carbon dioxide, while the molecular modeling of the coal matrix is only partially representative of a natural coal.

According to the original EPM model of Harris and Yung, the energy of interaction $U_{CO_2-CO_2}$ between two carbon dioxide molecules is:

$$U_{CO_2-CO_2} = \sum_{a=1}^{3}\sum_{b=1}^{3}\left(4\varepsilon_{ab}\left[\left(\frac{\sigma_{ab}}{r_{ab}}\right)^{12} - \left(\frac{\sigma_{ab}}{r_{ab}}\right)^{6}\right] + \frac{1}{4\pi\varepsilon_0}\frac{q_a q_b}{r_{ab}}\right) \tag{2}$$

where $(r_{ab})_{i,j=\{1,2,3\}}$ are the distances between two Lennard-Jones centers belonging to different molecules; σ_{ab} and ε_{ab} are the Lennard-Jones parameters for the interaction between atom a and atom b; q_a and q_b are the charges at the Lennard-Jones centers. The values of the parameters of the EPM model are given by Harris and Yung:[47] $\varepsilon_{\text{C-C}} = 28.129k_B$, $\sigma_{\text{C-C}} = 2.757$ Å, $\varepsilon_{\text{O-O}} = 80.507k_B$, $\sigma_{\text{O-O}} = 3.033$ Å, $\varepsilon_{\text{C-O}} = 47.588k_B$, $\sigma_{\text{C-O}} = 2.892$ Å, $q_{\text{C}} = -2q_{\text{O}} = 0.6512e$ and the distance between the carbon and oxygen atoms $L_{\text{C}-\text{O}} = 1.149$ Å.

The EPM model includes quadrupole-quadrupole interactions, whose range of interaction is larger than for the Lennard-Jones potential: these interactions are proportional to r^{-5} in a first order expansion.[21] Nevertheless, we applied a cutoff radius of 23 Å. This approximation is valid since the energy which is not taken into account is negligible. Indeed, for pure carbon dioxide at a fugacity of 7 MPa, the electrostatic energy calculated by using this cutoff radius differed from the energy calculated with the Ewald sum[21,22] by less than 1%.

Using the EPM model for CO_2, we performed a series of simulations of bulk CO_2 and computed its density and pressure at a temperature $T = 310$ K. The results are displayed in Figure 2 together with an experimental equation of state for CO_2 proposed by Span and Wagner.[48] The EPM model captures well the experimental behavior for subcritical and supercritical pressures. Near the critical pressure $P_{cr} = 7.4$ MPa, the EPM model somewhat differs from the experimental values. The discrepancy observed between the experimental values and those calculated with the EPM model comes from the fact that the temperature considered, $T = 310$ K, is near the critical

temperature $T_{cr} = 304$ K for CO_2, while the rigid EPM model was not developed originally to be used in supercritical conditions. Compared to other existing molecular models,[49,50] this model is not necessarily the most accurate to simulate carbon dioxide at temperatures and pressures representative of underground conditions. But it is one of the most representative for the underlying physics of the interactions, which is crucial for the simulation of adsorption.

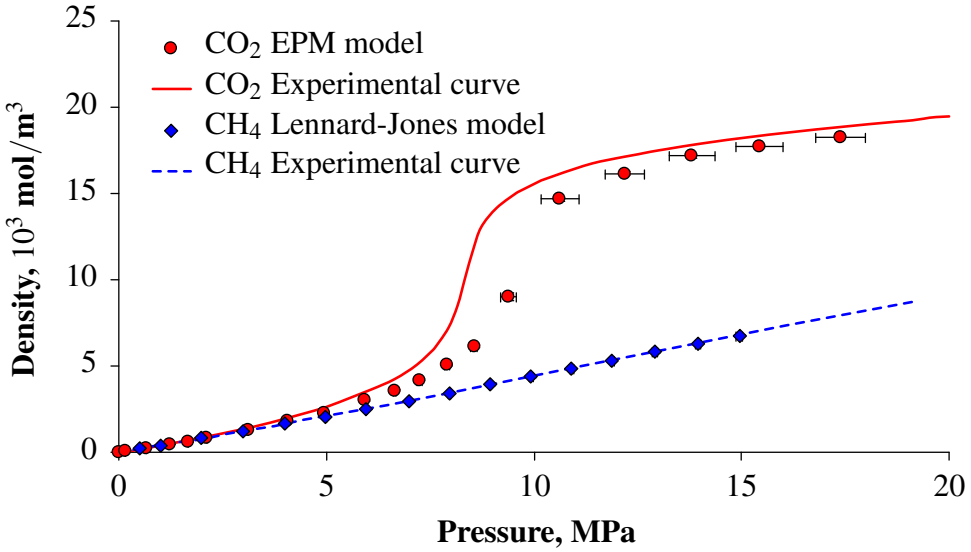

Figure 2: Equation of state for CH_4 and CO_2 at a temperature $T = 310$ K: molecular models and experimental curves.[46,48]

Methane - Carbon dioxide interactions

We modeled the intermolecular interaction between methane and carbon dioxide with Lennard-Jones potentials. The total inter-molecular energy of interaction between a molecule of methane and a molecule of carbon dioxide is:

$$U_{CH_4-CO_2} = \sum_{a=1}^{3} \left(4\varepsilon_{CH_4-a} \left[\left(\frac{\sigma_{CH_4-a}}{r_{CH_4-a}} \right)^{12} - \left(\frac{\sigma_{CH_4-a}}{r_{CH_4-a}} \right)^{6} \right] \right) \tag{3}$$

where σ_{CH_4-a} and ε_{CH_4-a} are the Lennard-Jones parameters for the interaction of methane with atom a (carbon or oxygen) of carbon dioxide. These parameters are derived from the Lennard-Jones parameters of the molecular model for pure methane and pure carbon dioxide following the Lorentz-Berthelot rules:[21] $\sigma_{CH_4-a} = \frac{1}{2}(\sigma_a + \sigma_{CH_4})$ and $\varepsilon_{CH_4-a} = \sqrt{\varepsilon_a \varepsilon_{CH_4}}$.

Prior to the simulation of mixture adsorption, we performed simulations of the CO_2-CH_4 bulk mixture in the isobaric-isothermal ensemble for the five sets of temperature and pressure and for mixture compositions ranging from pure methane to pure carbon dioxide. We computed the fugacities of each fluid with the Widom insertion method.[22] The results are displayed in Figure 3. We used these values of fugacities for the adsorption simulations of the mixture in the grand canonical ensemble.

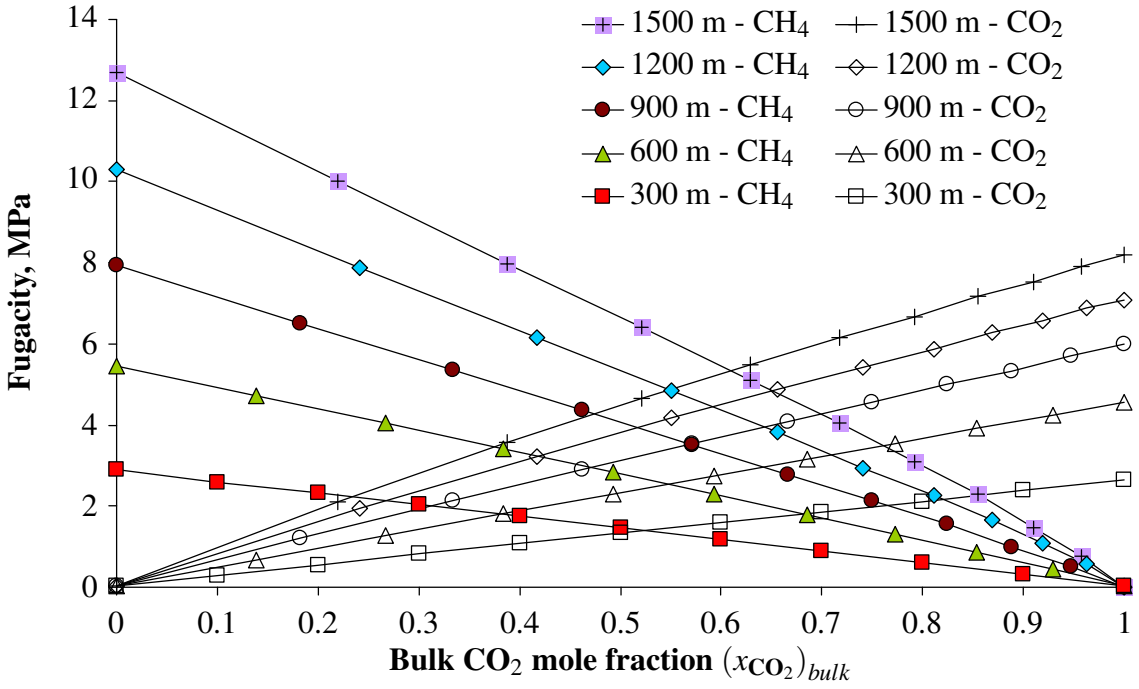

Figure 3: Fugacities of methane and carbon dioxide in function of the mixture composition for the various geological depths considered.

Fluid - coal interactions

In this work, we assumed that adsorption of methane and carbon dioxide in coal did not occur through chemical adsorption. This assumption is supported by the fact that the heats of adsorption of carbon dioxide and methane in coal, either measured by calorimetry experiments[7] or estimated from experimental adsorption isotherms,[7,25,51] are quite small (≈ 25 kJ/mol) which corresponds to physical adsorption. Nevertheless, detailed scanning calorimetry indicates that the first molecules of carbon dioxide adsorbed might be chemically bonded.[52] Following the assumption of physical

adsorption, the interactions between the CS1000 matrix and the fluids only involve the following types of interactions: steric repulsion, London dispersion forces, electrostatic interaction for carbon dioxide, and induced electrostatic interaction for methane.

Carbon dioxide

The molecule of carbon dioxide exhibits a quadrupole electrostatic moment, which makes the molecule sensitive to any electrostatic field in the surrounding of the CS1000 matrix. To account for this electrostatic interaction, we modeled the electrostatic field generated by the quantum charge distribution in CS1000 with point charges at the center of the carbon and hydrogen atoms of CS1000. The use of point charge for the representation of the CS1000 electrostatic field is convenient because of its simplicity. At the atomic scale however, charges are not localized in the matter but distributed in space according to the quantum mechanics wave functions. The point charges are chosen such that the electrostatic field in the vicinity of an adsorbed fluid molecule is similar to the electrostatic field that could be calculated with quantum mechanics. For large systems however (in particular for the CS1000 sample) quantum mechanics calculations become prohibitive and it is necessary to use approximate methodologies which provide a rough estimate of the point charges distribution. Among other possibilities, we chose the 'partial equalization of orbital electronegativity'.[53] With this method the charges on the carbon and hydrogen atoms ranged from $-0.15e$ to $0.15e$.

The steric repulsion and the London dispersion forces can be modeled with Lennard-Jones potentials. A Lennard-Jones potential was used by Jain et al. [40] to simulate the adsorption of argon in CS1000. Thus we modeled the carbon dioxide - CS1000 interaction potential with a Lennard-Jones potential and with point charges interactions:

$$U_{\mathrm{CO_2-CS1000}}(\mathbf{r}) = \sum_{i\in \mathrm{CS1000}} \sum_{a=1}^{3} \left(4\varepsilon_{ai} \left[\left(\frac{\sigma_{ai}}{r_{ai}} \right)^{12} - \left(\frac{\sigma_{ai}}{r_{ai}} \right)^{6} \right] + \frac{1}{4\pi\varepsilon_0} \frac{q_a q_i}{r_{ai}} \right) \tag{4}$$

where $(r_{ai})_{a=\{1,2,3\}}$ are the distances between the Lennard-Jones centers of the EPM model and the atom a (carbon or hydrogen) of CS1000; σ_{ai} and ε_{ai} are the appropriate Lennard-Jones parameters

for the interaction between atom i of CS1000 and center a of the EPM model; q_i and q_a are the point charges on an atom i of CS1000 and on a center a of the EPM model.

The Lennard-Jones parameters σ_{ai} and ε_{ai} are obtained following the Lorentz-Berthelot rules: $\sigma_{ai} = \frac{1}{2}(\sigma_a + \sigma_i)$ and $\varepsilon_{ai} = \sqrt{\varepsilon_a \varepsilon_i}$ where a stands for a center of the EPM model and i stands for a carbon or hydrogen atom of CS1000. σ_a and ε_a are the parameters used for the EPM model. For the carbon and hydrogen atoms of CS1000, we used the values of Jain et al.:[40] $\sigma_{\mathrm{C}} = 3.36$ Å, $\varepsilon_{\mathrm{C}} = 28 \cdot k_B$, $\sigma_{\mathrm{H}} = 2.42$ Å and $\varepsilon_{\mathrm{H}} = 15.08 \cdot k_B$.

Like for pure carbon dioxide, we imposed a cutoff radius: for distances larger than 23 Å we set the electrostatic interaction to zero. The range of the electrostatic interaction is larger than the range of interaction of the Lennard-Jones potential, but we checked that the use of a cutoff radius is valid: on a sample of molecular configurations of CO_2 adsorbed in CS1000, the electrostatic energy calculated with the Ewald sum method[21,22] or by introducing a cutoff radius differed by less than 1%.

Methane

We modeled the interaction of methane with CS1000 with the Lennard-Jones model:

$$U_{\mathrm{CH_4-CS1000}}(\mathbf{r}) = \sum_{i \in \mathrm{CS1000}} 4\varepsilon_{i-\mathrm{CH_4}} \left(\left(\frac{\sigma_{i-\mathrm{CH_4}}}{r_{i-\mathrm{CH_4}}} \right)^{12} - \left(\frac{\sigma_{i-\mathrm{CH_4}}}{r_{i-\mathrm{CH_4}}} \right)^{6} \right) \tag{5}$$

where the parameters $\sigma_{i-\mathrm{CH_4}}$ and $\varepsilon_{i-\mathrm{CH_4}}$ are the appropriate Lennard-Jones parameters, which depend on the nature of the atom i (carbon or hydrogen). These parameters are obtained following the Lorentz-Berthelot rules: $\sigma_{i-\mathrm{CH_4}} = \frac{1}{2}(\sigma_i + \sigma_{\mathrm{CH_4}})$ and $\varepsilon_{i-\mathrm{CH_4}} = \sqrt{\varepsilon_i \varepsilon_{\mathrm{CH_4}}}$. The Lennard-Jones parameters $\sigma_{\mathrm{CH_4}}$ and $\varepsilon_{\mathrm{CH_4}}$ are those used for the model of pure methane, and the values of the Lennard-Jones parameters for the carbon and hydrogen atoms of CS1000 are the same values as for the interactions between carbon dioxide and CS1000: $\sigma_{\mathrm{C}} = 3.36$ Å, $\varepsilon_{\mathrm{C}} = 28 \cdot k_B$, $\sigma_{\mathrm{H}} = 2.42$ Å, and $\varepsilon_{\mathrm{H}} = 15.08 \cdot k_B$.

The energy of the induced electrostatic interaction[54] between methane and CS1000 is negligible compared to the Lennard-Jones potential for most of the inter-particle distances r. Only for

inter-particle distances r around σ_{C-CH_4}, for which the Lennard-Jones potential is equal to zero, is the induced electrostatic interaction non negligible. Since this range is very small, we neglected the induced electrostatic energy in our simulations.

Size of the simulation box

The size of the CS1000 model is $25 \times 25 \times 25$ Å^3. A simulation box of this size would be too small to simulate the fluids, for which the cutoff radii were chosen at 23 Å. So we simulated adsorption in a simulation box twice as large in each direction (i.e., $50 \times 50 \times 50$ Å^3) made by juxtaposing eight replicas of the CS1000 model. Since CS1000 has been developed with periodic boundary conditions, we introduced no discontinuity by doing so and the resulting solid remained chemically stable.

A simulation box of $50 \times 50 \times 50$ Å^3 is large enough to be representative of the system we intend to simulate. Indeed, small angle X-Ray scattering experiments were performed on the porous carbon we considered and are at the heart of the reconstruction technique that led to the molecular model we use.[37] These experiments show that the molecular structure of this material has no characteristic features larger than about 1 nm. The same experiment performed on char leads to the same conclusion.[55]

Results and discussion

This section presents the results of the adsorption simulations performed.

Adsorption isotherms in micropores

Total amounts adsorbed

We simulated adsorption of the CO_2-CH_4 mixture in the CS1000 micropores. An example of simulated state is displayed in Figure 4. The total amount of methane and carbon dioxide in

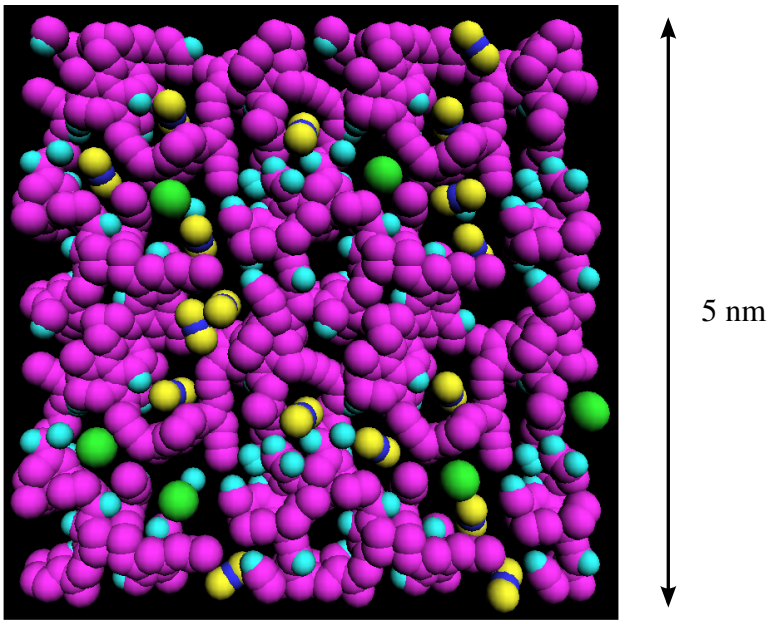

Figure 4: Example of molecular configuration sampled for the adsorption of a mixture of CO_2 and CH_4 in the CS1000 sample. The molecules of CO_2 are in yellow and dark blue, the molecules of CH_4 are in green, the carbon and hydrogen atoms of CS1000 are in pink and light blue.

micropores per unit volume of CS1000 was computed and is displayed in Figure 5. In this work we computed the amounts over 10^7 Monte Carlo steps which led to precise results when simulating pure component adsorption (Figure 7) but is insufficient to reach a similar precision for mixture adsorption (Figure 5). As expected, carbon dioxide adsorbed preferentially to methane: the total amount of carbon dioxide in CS1000 exceeded that of methane for a bulk CO_2 mole fraction as small as 0.25. We also observe that the total amounts adsorbed did not evolve significantly with the depth of the injection site considered, although a slight trend could be identified: the amount of adsorbed methane increased slightly with the depth of the site, whereas the amount of adsorbed carbon dioxide decreased slightly.

The selectivity, also called separation factor, is a criterion to assess the performance of the CS1000 sample to preferentially adsorb carbon dioxide in a mixed CO_2-CH_4 atmosphere. The carbon dioxide selectivity S_{CO_2} is defined as:[56,57]

$$S_{CO_2} = \left(\frac{x_{CO_2}}{x_{CH_4}}\right)_{\text{CS1000}} \Big/ \left(\frac{x_{CO_2}}{x_{CH_4}}\right)_{bulk} \tag{6}$$

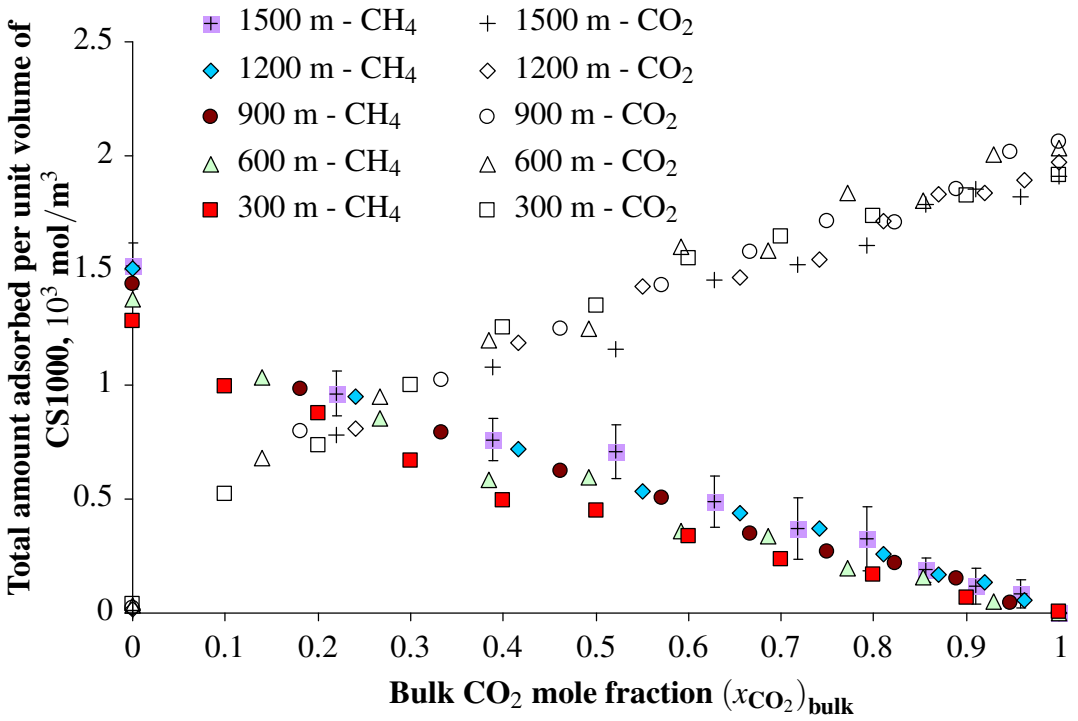

Figure 5: Total amounts of CO_2 and CH_4 adsorbed in a CS1000 sample exposed to a mixture of CO_2-CH_4 for the various geological depths considered. For sake of clarity we displayed the uncertainties for one of the curves only (estimation with the block averaging method).

where x_{CO_2} and x_{CH_4} are the mole fractions of carbon dioxide and of methane, respectively. The subscript $\square_{bulk}$ means that the mole fractions are those in the bulk, whereas the subscript $\square_{CS1000}$ means that the mole fractions are those in the CS1000 sample.

We calculated the selectivity of carbon dioxide in CS1000: the results are displayed in Figure 6. The selectivity was always greater than unity, meaning that, at all temperatures and pressures here considered, carbon dioxide was adsorbed preferentially to methane. Two trends are observed: the deeper the reservoir considered was, the lower the selectivity was; and the higher the CO_2 mole fraction was, the lower the selectivity was. The fact that the selectivity decreased with the depth means that, for the same amount of methane recovered, less carbon dioxide is sequestered in deep injection sites than in shallow ones.

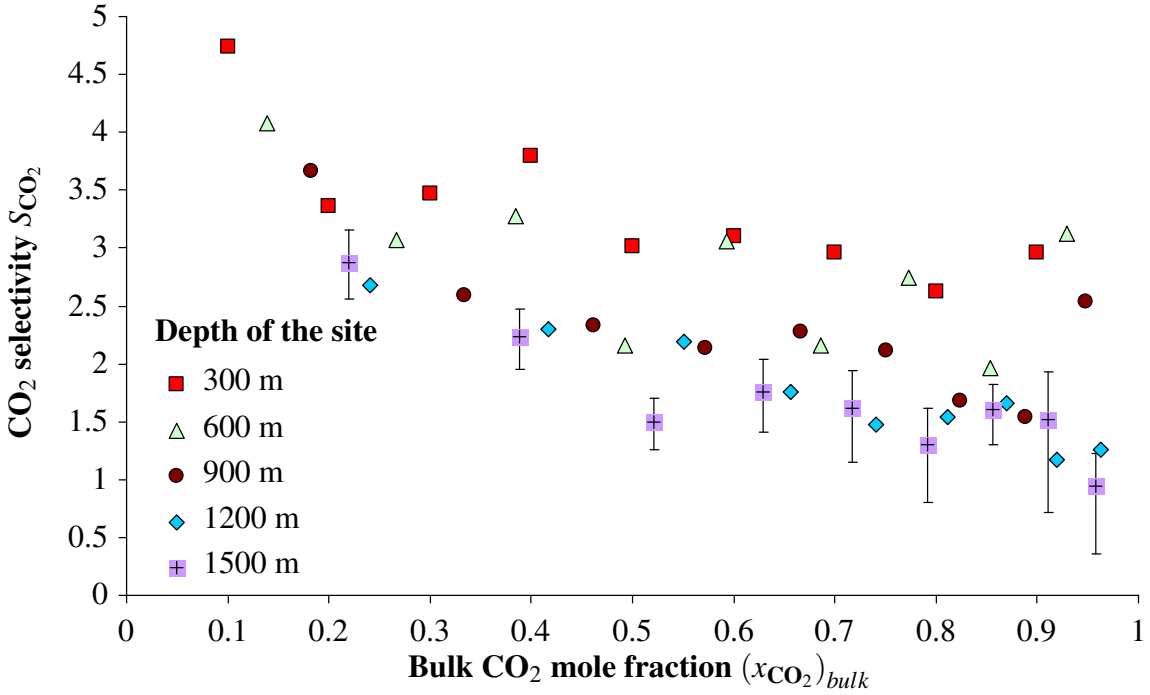

Figure 6: Selectivity of CO_2 in the CS1000 sample. For sake of clarity we displayed the uncertainties for one of the curves only.

Amounts adsorbed in excess

Ottiger et al. [9] have performed laboratory experiments of CO_2-CH_4 mixture adsorption in coal. Our results cannot be directly compared to these experiments because the adsorbed amount measured

by Ottiger et al. are excess amounts: The increase in mass of the coal sample immersed in the fluid which is measured is not the total mass of fluid in the solid but, because of the buoyancy, is the mass of fluid adsorbed in excess of the mass of bulk fluid. The excess amount adsorbed is the total amount adsorbed minus the amount that would occupy the microporosity if the fluid mixture was at its bulk density in the micropores.

Calculating excess amounts adsorbed in micropores from total amounts requires the knowledge of the volume of micropores. A possible estimate of the volume of micropores in CS1000 is the volume occupied by the maximum amount of fluid adsorbed at high pressure, assuming that the fluid is at a liquid density. The maximum amount of carbon dioxide adsorbed in micropores was around 155 molecules in the $50 \times 50 \times 50$ Å^3 CS1000 sample and was reached for a bulk pressure of 9 MPa. The volume of micropores was estimated with the volume occupied by the same amount of molecules at a liquid density. The liquid density of carbon dioxide at 260 K is between 2.29×10^4 mol/m^3 at a pressure $P = 4$ MPa and 2.43×10^4 mol/m^3 at a pressure $P = 20$ MPa. Thus we could estimate the volume of micropores to $155 \big/ \left(2.35 \times 10^4 \cdot \mathcal{N}_A\right) \approx 1.1 \times 10^4$ nm^3 in a total volume of porous solid of 1.25×10^5 nm^3, which corresponds to a porosity of 9%. The same calculation with the maximum amount of methane adsorbed (around 115 molecules) and considering a methane liquid density of 2.56×10^4 mol/m^3 at a temperature $T = 120$ K yielded a porosity of 6%. An alternative estimate of the volume of micropores is the 'geometric porosity', i.e., the volume that can be occupied by a hard sphere of given size, considering the first Lennard-Jones parameter σ as geometric border of the solid atoms. By doing so, the geometric porosity probed by a hard sphere with a 3Å diameter was estimated to 14%, which is greater than the previous estimates of the volume of micropores obtained by other means. The difference is due to the fact that the whole geometric porosity cannot be fully filled with a set of fluid molecules and to the fact that the fluid molecules we considered are larger than a sphere with a 3 Å diameter: the Van der Waals radius of methane is 3.751 Å and that of carbon dioxide is 5.331 Å in the direction of the oxygen atoms and 3.033 Å in the normal direction. Therefore, it is clear that defining a volume of micropores at the molecular scale is not straighforward. The first two estimates (6% and 9%) are

equally valid. The geometrical porosity (14%) is not a realistic value but stands for an upper bound of the actual porosity. In any case, given the equations of state of the fluid considered, the bulk densities, and therefore the micropore volume, only become significant at pressures greater than 6 or 7 MPa. The excess amount estimated with a microporosity of 9% is significantly lower than the amount estimated with a porosity of 6%. The relative difference between the two estimates is 10% at 8 MPa for both CH_4 and CO_2 and this relative difference increases with the pressure. For lower pressures, whatever the micropore volume chosen, the excess amount adsorbed was nearly equal to the total amount adsorbed. In volume per unit mass, these estimates corresponded to porosities of 0.040 and 0.060 cm^3/g, respectively, which is consistent with the volume of micropores of 0.072 cm^3/g estimated by Ottiger et al..[58]

In order to choose the value of microporosity, we compared the simulated excess isotherms of pure component adsorption to experimental ones, although the quantity measured in the laboratory experiment is the excess amount adsorbed in both micropores and mesopores. We considered the experimental results of Ottiger et al.[9] and we compared the pure CO_2 and pure CH_4 adsorption at 318.15 K. We display in Figure 7 this comparison. The value of microporosity used was 6%, which is the value that allowed the best fit between predicted isotherms and experimental ones. Although the amount of methane is slightly overestimated, the predicted and experimental curves exhibit similar trends, which suggests that most of the adsorption in natural coal takes place in micropores.

The excess amounts isotherms obtained at the different temperatures and pressures considered are displayed in Figure 8. The shape of the isotherms was similar to that of the total amount isotherms. The excess amount of adsorbed carbon dioxide was larger than the excess amount of adsorbed methane for bulk CO_2 mole fractions as small as 0.2. The excess amount of adsorbed carbon dioxide decreased with an increasing depth. The excess adsorbed amounts in conditions corresponding to sites at depths of 300 m and 600 m were very close to the total adsorbed amounts. However, at the three deepest sites considered, the excess adsorbed amounts were significantly lower than the total adsorbed amounts, because of the high bulk density of carbon dioxide for sites

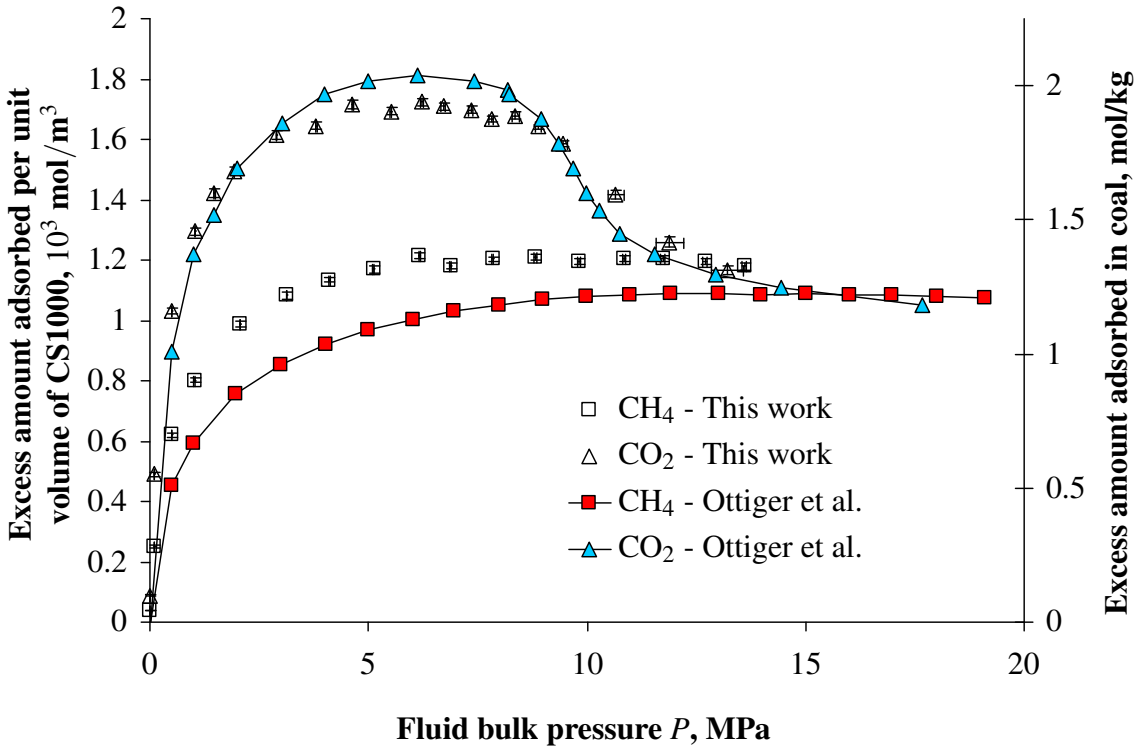

Figure 7: Excess amounts adsorbed estimated by molecular simulations in CS1000 micropores, and measured by Ottiger et al. [9] at 318.15 K. The uncertainties of our simulation results are represented but are too small to be clearly visible.

deeper than 800 m.

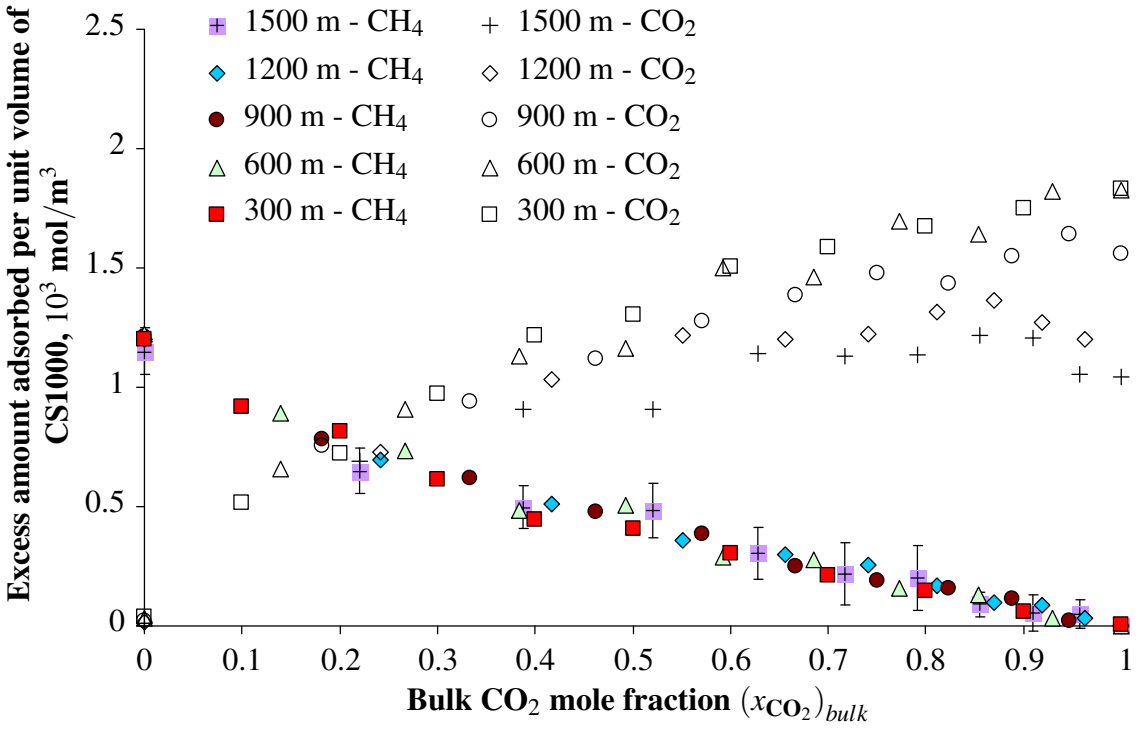

Figure 8: Excess amounts isotherms for the adsorption of the CO_2-CH_4 mixture in CS1000 for the various geological depths considered. For sake of clarity we displayed the uncertainties for one of the curves only.

The experimental isotherms adapted from Ottiger et al. [9] are displayed in Figure 9. One should note that Ottiger et al. [9] only varied the pressure of the mixture, while keeping the temperature constant and equal to 318.15 K. The adsorbed amounts at the five pressures we considered were obtained by linearly interpolating the data of Ottiger et al.. In addition, we display in Figure 10 the excess amounts estimated by molecular simulation together with those measured experimentally for sites at depths of 900 m and 1200 m, for which the temperature considered in the simulations and in the experiments are the closest. The comparison of the experimental isotherms with the isotherms computed by molecular simulation is quite satisfactory, although the amounts of methane were overestimated by the molecular simulations, as was the case for pure fluid adsorption (see Figure 7). Moreover, the excess amount of adsorbed CO_2 depends less on the pressure of the mixture (i.e., on the depth of the site of injection) experimentally than what could be inferred from the molecular simulations.

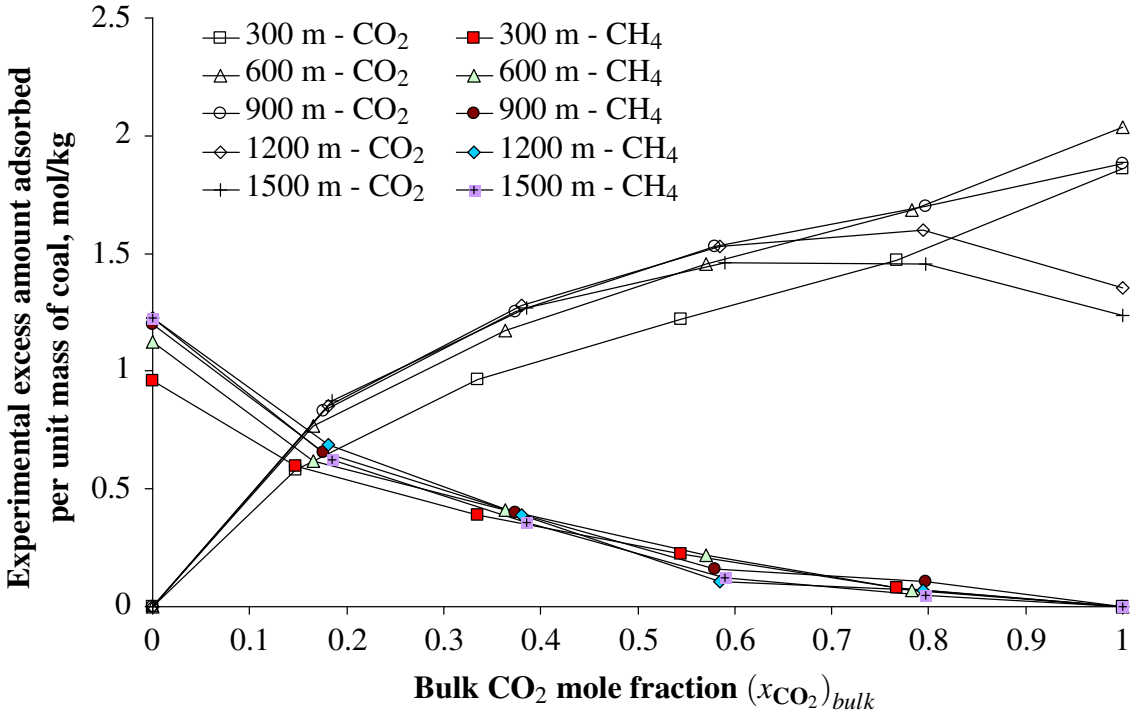

Figure 9: Experimental isotherms for the competitive adsorption of the CO_2-CH_4 mixture in coal at the various geological depths considered. Adapted from Ottiger et al..[9]

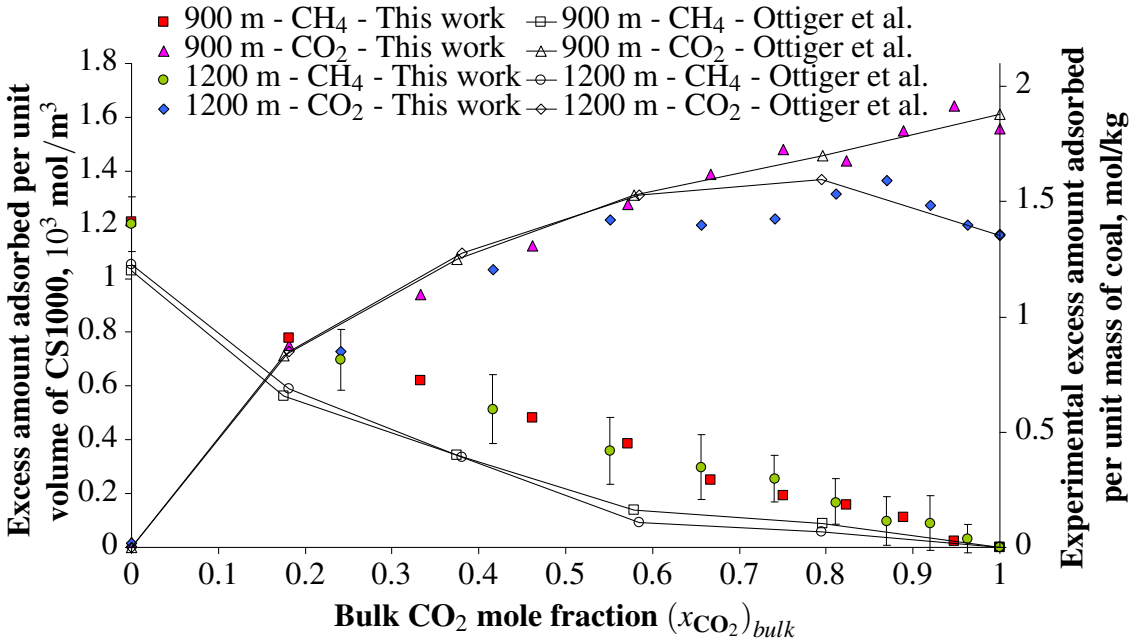

Figure 10: Excess amounts adsorbed estimated by molecular simulation and measured experimentally by Ottiger et al.[9] for the competitive adsorption of the CO_2-CH_4 mixture in coal at two of the geological depths considered. For sake of clarity we displayed the uncertainties for one of the curves only.

The following section is dedicated to predict the differential swelling induced by the progressive replacement of methane with carbon dioxide. We use a poromechanical model extended to micropore adsorption, which enables us to relate the adsorption isotherms to the differential swelling.

Adsorption induced differential swelling

Adsorption of fluids has an impact on the mechanical behavior of porous solids. To assess this impact, we developed in a recent work[19,20] a poromechanical model accounting for adsorption in micropores. In usual linearized poroelasticity,[59] the fluid entering the porous volume is assumed to be in its bulk state and the adsorption of fluid is not accounted for. The state equations, valid for a isotropic linear elastic macroporous medium (with pores larger than 50 nm) link the volumetric stress σ, the deviatoric stresses s_{ij}, and the change of porosity $\varphi = \phi - \phi_0$ (where ϕ is the actual porosity and ϕ_0 the porosity in the state of reference) to the volumetric strain ε, the deviatoric strains e_{ij}, and the fluid pressure P:

$$\begin{cases} \sigma = K\varepsilon - bP \\ \varphi = b\varepsilon + P/N \\ s_{ij} = 2Ge_{ij} \end{cases} \tag{7}$$

where K is the bulk modulus, G the shear modulus, b the Biot coefficient and N the Biot modulus. For an isotropic solid, the third equation relating the deviatoric stresses to the deviatoric strains remains unchanged when adsorption occurs. Accordingly we omit this last equation in the following developments.

For a mesoporous solid (with pores whose size is between 2 nm and 50 nm), the specific surface is important and a significant amount of the fluid molecules are not in their bulk state, but adsorbed at the surface of the pores. Vandamme et al.[13] extended usual poromechanics to account for surface effects. By introducing the fluid-solid interface energy γ and the specific surface s, the constitutive equations of poromechanics are modified as follows:

$$\begin{cases} \sigma - \widetilde{\sigma}_s \left.\frac{\partial s}{\partial \varepsilon}\right|_{\varphi=0} = K\varepsilon - b\left(P - \widetilde{\sigma}_s \left.\frac{\partial s}{\partial \varphi}\right|_{\varepsilon=0}\right) \\ \varphi = b\varepsilon + \frac{1}{N}\left(P - \widetilde{\sigma}_s \left.\frac{\partial s}{\partial \varphi}\right|_{\varepsilon=0}\right) \end{cases} \tag{8}$$

where the quantity $\widetilde{\sigma}_s = \gamma + s \left.\frac{\partial \gamma}{\partial s}\right|_{T,\mu}$, introduced by Shuttleworth,[60] is called the interface stress. Such stress differs from the interface energy when this energy depends on the surface strain, which in general is the case for an interface involving a solid. At fixed temperature, the effect of surface adsorption on the interface energy (and on the interface stress) is predicted by the Gibbs' adsorption equation:[61]

$$d\gamma = -\sum_i \Gamma_i d\mu_i \tag{9}$$

where Γ_i are the excess amounts of fluid molecules adsorbed at the surface of the solid per unit area at the chemical potentials μ_i. Accordingly, making use of the constitutive equations (8) combined with the Gibbs adsorption equation (9), the mechanical behavior of a mesoporous solid subjected to surface adsorption is fully determined, provided the excess amount adsorbed at the pore surfaces are known.

When the size of the pores is of the order of the range of the molecular interactions (i.e., smaller than 2 nm when Van der Waals interactions are involved), all fluid molecules interact with the solid atoms and the notions of specific surface and even of pore volume become questionable. Brochard et al. [19,20] derived general poroelastic state equations, valid whatever the size of the pores:

$$\begin{cases} \sigma = K\varepsilon - \left.\frac{\partial}{\partial \varepsilon}\left(\int_0^p n\overline{V}_b dP\right)\right|_P \\ n = n(\varepsilon, P) \end{cases} \tag{10}$$

where n is the Lagrangian concentration of the fluid in the solid ($n = N/V_0$ where N is the amount of fluid molecules in the medium and V_0 is the volume of the undeformed porous medium), $n^0 = n(\varepsilon = 0, P)$ and $\overline{V}_b$ is the molar volume of the bulk fluid. The constitutive equations (10) are general and are consistent with usual poroelasticity (Equation 7) as well as with poroelasticity

extended to surface effects (Equation 8).[19,20]

How the fluid concentration n changes with strain can be complex and is very dependent on the commensurability of the size of the micropore to the size of the fluid molecules. In the case of amorphous solids with no specific pore size, molecular experiments on simple systems have shown that the fluid concentration depends linearly on the strain of the medium, and that the derivative $\partial n/\partial \varepsilon|_P$ is nearly proportional to the concentration at zero strain: $C = \partial n/\partial \varepsilon|_P / n^0$ is almost constant. We call C the coupling coefficient. Accordingly, the first constitutive equation (10) can be simplified as follows:

$$\sigma = K\varepsilon - C\int_0^p n^0 \overline{V}_b dP \tag{11}$$

For the coal tested by Ottiger et al.,[9,58] for which $K = 2.65$ GPa, the coupling coefficient is equal to $C_{CH_4} = 6.05 \pm 7\%$ for methane and to $C_{CO_2} = 7.60 \pm 20\%$ for carbon dioxide.[19,20]

According to equation (11), the strain ε^u of a coal sample immersed in a fluid (in which case $\sigma = -P$) is related to the amount n^0 of fluid adsorbed at zero strain:

$$\varepsilon^u(P) = -\frac{P}{K} + \frac{C}{K}\int_0^P n^0 \overline{V}_{bulk} dP \tag{12}$$

By using this equation with the values of coupling coefficients and bulk modulus given above, we estimated the swelling of a coal sample immersed in pure methane and pure carbon dioxide. We display in Figure 11 the results of our calculation together with the measurements performed by Ottiger et al..[9] The swelling estimated with the poromechanical equation (12) together with the adsorption isotherms obtained by molecular simulation is consistent with the experiments. At pressures lower than 2 MPa, the swelling was overestimated for both fluids. Such a discrepancy is due to the fact that the coupling coefficients C_{CH_4} and C_{CO_2} are overestimated for pressures lower than 2 MPa.[19,20] Experimentally, adsorption-induced contractions of porous carbons are measured at low pressures.[62,63] Such contractions correspond to negative values of the coupling coefficient. At fluid pressures larger than 2 MPa, because of the integral form of equation (12), the initial over-

estimation is propagated. Nevertheless, the swellings estimated with the poromechanical model combined with the simulated adsorption isotherms followed evolutions very similar to those of the swellings measured experimentally.

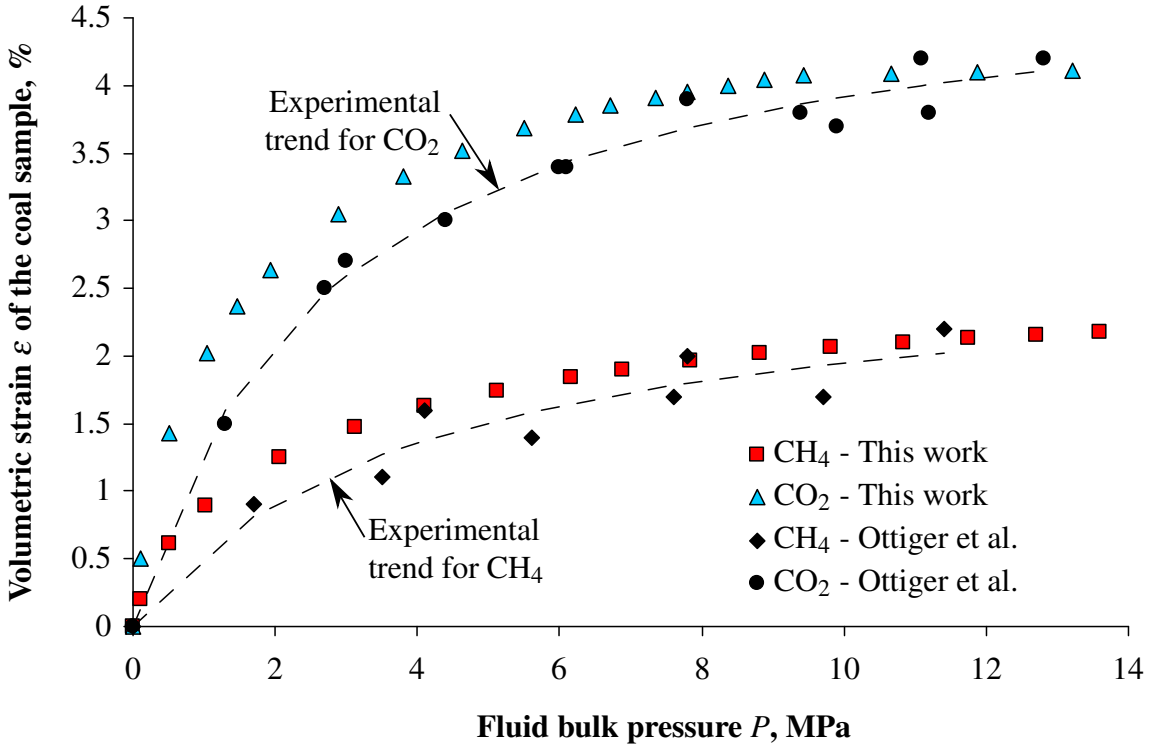

Figure 11: Swelling of a coal sample immersed in a fluid, measured experimentally and estimated with the poromechanical model combined with adsorption isotherms obtained by molecular simulations. The experimental data are from Ottiger et al..[9]

For fluid mixtures the first constitutive equation in the set of equations (10) becomes:

$$\sigma = K\varepsilon - \frac{\partial}{\partial \varepsilon}\left(\int_{(-\infty,\ldots,-\infty)}^{(\mu_1,\ldots,\mu_n)} \sum_i n_i(\varepsilon,\mu_1,\ldots,\mu_n)\, d\mu_i \right)\Bigg|_{\mu_1,\ldots,\mu_n,e_{ij}=0} \tag{13}$$

where the n_i and μ_i are the molar concentrations and molar chemical potentials of the different components of the mixture. The integration does not depend on the path chosen. Assuming that, for fluid mixtures, the fluid concentrations are linear with strain and that the corresponding coupling coefficients $C_i = \partial n_i/\partial \varepsilon|_{\mu_1,\ldots,\mu_n} \Big/ n_i^0$ are constant, the first constitutive equation becomes:

$$\sigma = K\varepsilon - \int_{(-\infty,...,-\infty)}^{(\mu_1,...,\mu_n)} \sum_i C_i n_i^0 (\mu_1, ..., \mu_n) \, d\mu_i \tag{14}$$

At given bulk pressure of the fluid mixture, the replacement of methane with carbon dioxide in coal corresponds to specific values of chemical potentials which depend on the bulk CO_2 mole fraction $(x_{CO_2})_{bulk}$. The corresponding fugacities are displayed in Figure 3. Comparing a coal sample exposed to a mixture of CO_2 and CH_4 with a coal sample exposed to a fluid at the same pressure as the mixture but made of pure methane, the variation $\Delta\sigma$ of volumetric stress, the variation $\Delta\varepsilon$ of volumetric strain and the adsorbed amounts are related according to:

$$\Delta\sigma = K\Delta\varepsilon - \int_{\left(\mu_{CH_4}^{pure},-\infty\right)}^{\left(\mu_{CH_4}(x_{CO_2}),\mu_{CO_2}(x_{CO_2})\right)} \left(C_{CH_4} n_{CH_4}^0 d\mu_{CH_4} + C_{CO_2} n_{CO_2}^0 d\mu_{CO_2}\right) \tag{15}$$

The so-called differential swelling ε_{diff} is the variation of volumetric strain when the volumetric stress is constant (i.e., when $\Delta\sigma = 0$). This differential swelling is not the swelling that would be observed in situ, since in a coal bed reservoir the coal matrix is not free to swell. Nevertheless, the differential swelling quantifies the mechanical effect induced by adsorption. From equation (15), the differential swelling ε_{diff} can be expressed as:

$$\varepsilon_{diff} = \frac{1}{K} \int_{\left(\mu_{CH_4}^0,\mu_{CO_2}^0\right)}^{\left(\mu_{CH_4},\mu_{CO_2}\right)} \left(C_{CH_4} n_{CH_4}^0 (\mu_{CH_4}, \mu_{CO_2}) \, d\mu_{CH_4} + C_{CO_2} n_{CO_2}^0 (\mu_{CH_4}, \mu_{CO_2}) \, d\mu_{CO_2}\right) \tag{16}$$

The amounts $n_{CH_4}^0 (\mu_{CH_4}, \mu_{CO_2})$ of adsorbed methane and $n_{CO_2}^0 (\mu_{CH_4}, \mu_{CO_2})$ of adsorbed carbon dioxide are known from the adsorption simulations performed (see Figure 5). Using equation (16), we estimated the differential swelling of the coal matrix consecutive to a progressive replacement of methane with carbon dioxide. We display in Figure 12 the differential swelling estimated for coal beds in sites at various depths. The strain depended concavely on the bulk CO_2 mole fraction: almost half of the differential swelling was achieved for a bulk CO_2 mole fraction of 0.2. According to this result, the differential swelling occurs at the early stage of the injection process.

The differential swelling was mostly independent of the injection site depth, although for bulk CO_2 mole fractions below 0.7 the differential swelling was smaller at the shallowest sites considered, while for bulk CO_2 mole fractions above 0.8 the differential swelling was smaller at the deepest sites considered.

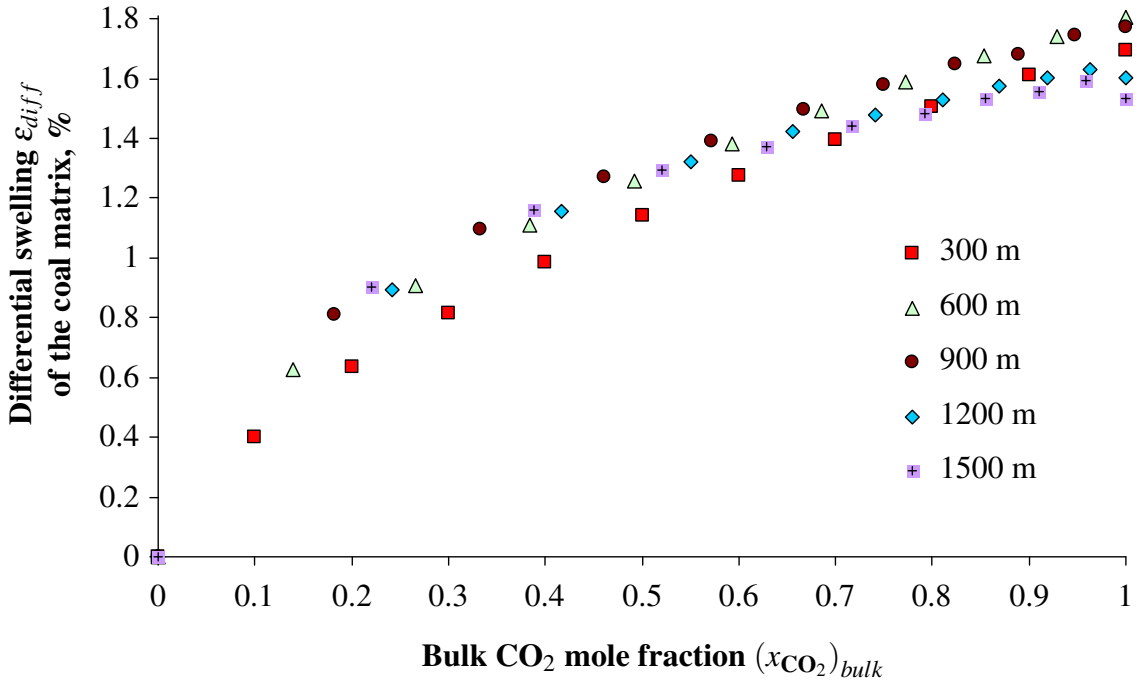

Figure 12: Differential swelling of the coal matrix estimated for the different site depths considered.

We display in Figure 13 the estimated differential swelling in function of the CO_2 mole fraction in CS1000: the differential swelling was almost proportional to the CO_2 mole fraction in CS1000. The swelling in conditions corresponding to a site depth of 300 m was slightly lower than for conditions corresponding to sites at other depths, except for $(x_{CO_2})_{CS1000} > 0.9$. In practice, for field application, this proportional relationship between differential swelling and CO_2 mole fraction in coal could help to estimate quickly the differential swelling of the coal matrix.

Discussion

Our results suggest that there is no optimal depth to limit the differential swelling induced by an injection of CO_2. But how this swelling impacts the permeability of coal in underground conditions

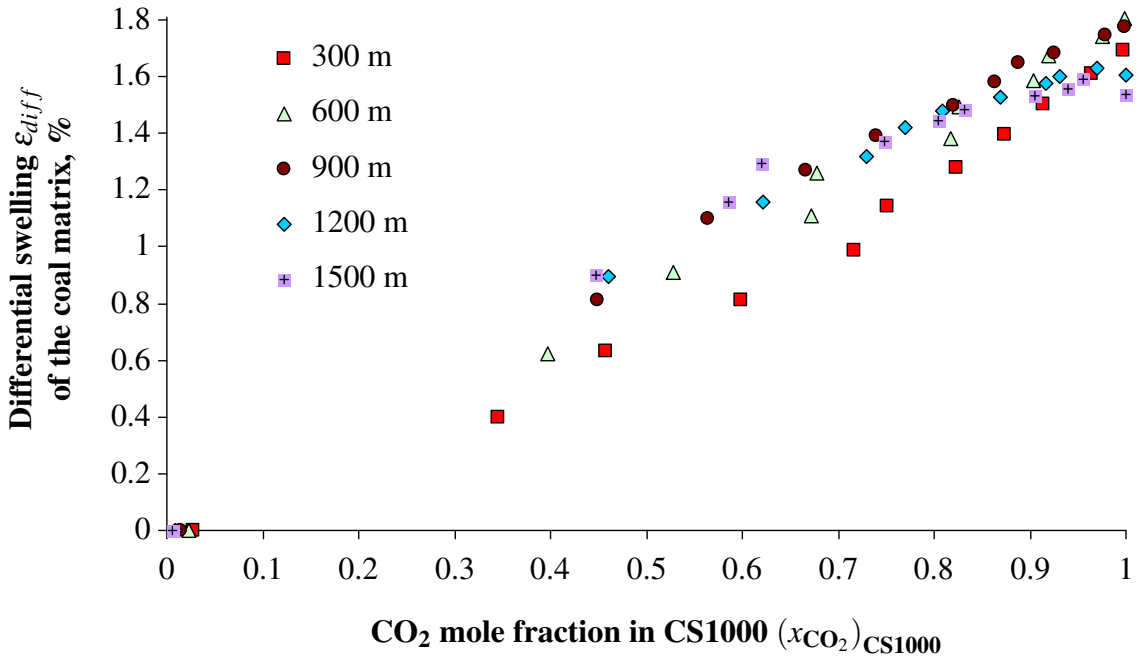

Figure 13: Differential swelling of the coal matrix in function of the CO_2 mole fraction in CS1000.

is a complex question. The prediction of the permeability loss in a coal seam requires an appropriate permeability model to be developed. Although the differential swelling is almost insensitive to the depth, how this swelling will lead to a decrease of the permeability of the reservoir may well depend on the underground stresses and therefore on the depth. All the differential strain curves predicted have to be considered carefully since the results of the molecular simulations are not results of laboratory experiments. We discuss hereafter the main approximations of our modeling.

1. In our simulations, all micropores are accessible because of the random insertion trials in the grand canonical Monte Carlo method. In natural coal, the microporous network is imperfectly connected and exhibits numerous constrictions which limit the accessibility of the fluid molecules to the micropore space.[64] To enter a micropore, an energy barrier may need to be overcome: the diffusion is said to be 'activated'. The activation energy is not the same for methane and for carbon dioxide.[65,66] Some micropores are likely to remain inaccessible to both methane and carbon dioxide. However, there exists other micropores that are accessible to carbon dioxide but remain closed for methane. Bae et al. [66] estimated the volume of those latter micropores from the adsorption-desorption hysteresis: for the two coals

they considered, 13% and 17% of the total volume of micropores presented a constricted access. In our simulation results, the underestimation of the relative difference between the amounts of carbon dioxide and of methane adsorbed (which is of about 15%) could therefore be explained by the fact that Monte Carlo simulations provide access to all micropores.

2. Oxygen atoms are not accounted for in the CS1000 model, whereas in natural coal oxygen amounts to about 10% of the total mass. Oxygen atoms significantly infuence the distribution of charge in a molecular structure because of their high electronegativity. For methane, we showed that the induced electrostatic interactions are small compared to the dispersion forces and steric repulsion. However, electrostatic interactions are significant for the adsorption of carbon dioxide. One can expect that higher electrostatic interactions with the solid skeleton favor specific orientations of the carbon dioxide molecules and may enhance the adsorption by lowering the total energy of interaction with the solid. Tenney and Lastoskie [36] simulated the adsorption of carbon dioxide on pure carbon surfaces and on carbon surfaces with chemical heterogeneities characteristic of coal: comparing this latter case with the former, the adsorption of carbon dioxide is enhanced in most cases but not always, adsorption occurs at lower pressures, and the maximum amount adsorbed increases, on average, by 5%. Therefore, the absence of oxygen is a drawback of our modeling. The error associated to this absence is somewhat difficult to quantify, but can be estimated to 5% in first order.

3. Liquid water is commonly present in coal seams and is known to affect the injection process. Water molecules are adsorbed in micropores only on hydrophilic sites.[7] Therefore, water contributes to the adsorption-induced swelling of coal. Moreover, the access to the micropores and the amount of stored carbon dioxide are reduced in presence of water. In this work, we only considered the adsorption of carbon dioxide and methane and we did not account for the effect of the presence of water. For field application, this effect cannot be ignored.

4. We did not consider the possible hysteresis of the adsorption and the desorption processes.

However, adsorption of carbon dioxide and methane in coal may present hystereses.[51,66,67] The observed hystereses are generally small. Moreover, their physical origin is unclear. Potential origins for such hystereses are: chemical adsorption, constricted diffusion, insufficient equilibration of the samples, and so on. On the other hand, other experimental studies did not report any hysteresis.[8,58]

Therefore, the modeling we proposed to assess the differential swelling of coal in underground conditions has a few limitations. In dry conditions, i.e., in the absence of water, and for site deeper than 200 m such a modeling should give relevant predictions with an accuracy of $\pm 15\%$. However, in order to apply the modeling the values of the coupling coefficients $C_{\mathrm{CH_4}}$ and $C_{\mathrm{CO_2}}$ for the coal considered should be determined experimentally with the analysis developped by Brochard et al..[19,20] For shallow injection site (< 200 m), however, our modeling is not reliable since the poromechanical model overestimates the adsorption-induced swelling at low pressures ($P < 2$MPa). The major drawback for field application is the fact that this model does not account for the presence of water whereas in most cases coal beds are filled with water.

The main shortcomings of our modeling could be overcome by developing a more realistic molecular model of coal in which oxygen atoms are accounted for. To do so the reverse Monte Carlo method of Jain et al. [39] can be adapted with a reactive inter-atomic potential accounting for Oxygen atoms. With such a molecular model of coal, the adsorption of water can be simulated. In addition, the poromechanical model should be adapted to the presence of water, which is not miscible with carbon-dioxide.

Conclusions

In this work we simulated competitive adsorption of carbon dioxide and methane in CS1000, a realistic model for microporous coal. Competitive adsorption of the two fluids in the coal micropores is responsible for the differential swelling phenomenon, a major problem for field application of ECBM. The progressive replacement of methane by carbon dioxide in a coal seam was simulated,

at various temperatures and mixture bulk pressures corresponding to five different underground site depths between 300 m and 1500 m. Comparison with experimental isotherms was satisfactory. The adsorption isotherms were used in a poromechanical model accounting for adsorption in micropores to assess the induced differential strain. The predicted strain curves suggested that the coal swelling problem appears at low CO_2 mole fractions (as low as 0.2), i.e. at early stages of injection. The adsorption induced swelling was almost insensitive to the depth of the injection site and was proportional to the CO_2 mole fraction in the coal.

References

(1) Jenkins, C.; Boyer, C. *Journal of Petroleum Technology* **2008**, *60*, 92–99.

(2) Mazumder, S.; Wolf, K. H. *International Journal of Coal Geology* **2008**, *74*, 123 – 138.

(3) Pini, R.; Ottiger, S.; Burlini, L.; Storti, G.; Mazzotti, M. *Energy Procedia* **2009**, *1*, 1711–1717.

(4) Mazzotti, M.; Pini, R.; Storti, G. *The Journal of Supercritical Fluids* **2009**, *47*, 619–627.

(5) Reeves, S. The Coal-Seq Project: Key Results from Field, Laboratory, and Modeling Studies. *7th International Conference on Greenhouse Gas Control Technologies (GHGT-7)*, 2004.

(6) Metz, B.; Davidson, O.; de Coninck, H.; Loos, M.; Meyer, L. *Carbon Dioxide Capture and Storage*; Cambridge University Press, UK. pp 431., 2005.

(7) White, C. M.; Smith, D. H.; Jones, K. L.; Goodman, A. L.; Jikich, S. A.; LaCount, R. B.; DuBose, S. B.; Ozdemir, E.; Morsi, B. I.; Schroeder, K. T. *Energy & Fuels* **2005**, *19*, 659–724.

(8) Levine, J. R. *Geological Society, London, Special Publications* **1996**, *109*, 197–212.

(9) Ottiger, S.; Pini, R.; Storti, G.; Mazzotti, M. *Adsorption* **2008**, *14*, 539–556.

(10) Harpalani, S.; Schraufnagel, A. *Geotechnical and Geological Engineering* **1990**, *8*, 369–384.

(11) Bae, J.-S.; Bhatia, S. K. *Energy & Fuels* **2006**, *20*, 2599–2607.

(12) Balzer, C.; Wildhage, T.; Braxmeier, S.; Reichenauer, G.; Olivier, J. P. *Langmuir* **2011**, *27*, 2553–2560.

(13) Vandamme, M.; Brochard, L.; Lecampion, B.; Coussy, O. *Journal of the Mechanics and Physics of Solids* **2010**, *58*, 1489–1505.

(14) St. George, J. D.; Barakat, M. A. *International Journal of Coal Geology* **2001**, *45*, 105–113.

(15) Day, S.; Fry, R.; Sakurovs, R. *International Journal of Coal Geology* **2008**, *74*, 41–52.

(16) Pini, R.; Ottiger, S.; Storti, G.; Mazzotti, M. *Energy Procedia* **2009**, *1*, 1705–1710.

(17) Kowalczyk, P.; Ciach, A.; Neimark, A. V. *Langmuir* **2008**, *24*, 6603–6608.

(18) Gor, G. Y.; Neimark, A. V. *Langmuir* **2010**, *26*, 13021–13027.

(19) Brochard, L.; Vandamme, M.; Pellenq, R. J. M. submitted to JPMS.

(20) Brochard, L. Ph.D. thesis, Ecole des Ponts ParisTech, Université Paris Est, 2011.

(21) Allen, M. P.; Tildesley, D. J. *Computer Simulation of Liquids*; Oxford University Press, USA, 1989.

(22) Frenkel, D.; Smit, B. *Understanding Molecular Simulation*; Academic Press, Inc., 2001; p 638.

(23) Leach, A. R. *Molecular modelling : principles and applications*; Prentice Hall, 2001.

(24) Vassilev, S. V.; Vassileva, C. G. *Fuel Processing Technology* **1996**, *48*, 85–106.

(25) Glass, A. S.; Larsen, J. W. *Energy & Fuels* **1994**, *8*, 629–636.

(26) Bustin, R. M.; Clarkson, C. R. *International Journal of Coal Geology* **1998**, *38*, 3–26.

(27) Vassilev, S. V.; Kitano, K.; Vassileva, C. G. *Fuel* **1996**, *75*, 1537 – 1542.

(28) Özgen Karacan, C. *Energy & Fuels* **2003**, *17*, 1595–1608.

(29) Larsen, J. W.; Flowers, R. A.; Hall, P. J.; Carlson, G. *Energy & Fuels* **1997**, *11*, 998–1002.

(30) Takagi, H.; Maruyama, K.; Yoshizawa, N.; Yamada, Y.; Sato, Y. *Fuel* **2004**, *83*, 2427–2433.

(31) Steele, W. A. *Surface Science* **1973**, *36*, 317 – 352.

(32) Coasne, B.; Jain, S. K.; Naamar, L.; Gubbins, K. E. *Physical Review B* **2007**, *76*, 085416.

(33) Nguyen, T. X.; Bhatia, S. K.; Nicholson, D. *Langmuir* **2005**, *21*, 3187–3197.

(34) Do, D. D.; Nicholson, D.; Do, H. D. *The Journal of Physical Chemistry C* **2008**, *112*, 14075–14089.

(35) Vishnyakov, A.; Piotrovskaya, E. M.; Brodskaya, E. N. *Adsorption* **1998**, *4*, 207.

(36) Tenney, C.; Lastoskie, C. *Environmental Progress* **2006**, *25*, 343–354.

(37) Pikunic, J.; Clinard, C.; Cohaut, N.; Gubbins, K. E.; Guet, J.-M.; Pellenq, R. J.-M.; Rannou, I.; Rouzaud, J.-N. *Langmuir* **2003**, *19*, 8565–8582.

(38) Jain, S. K.; Pikunic, J. P.; Pellenq, R. J.-M.; Gubbins, K. E. *Adsorption* **2005**, *11*, 355–360.

(39) Jain, S. K.; Pellenq, R. J.-M.; Pikunic, J. P.; Gubbins, K. E. *Langmuir* **2006**, *22*, 9942–9948.

(40) Jain, S. K.; Gubbins, K. E.; Pellenq, R. J.-M.; Pikunic, J. P. *Carbon* **2006**, *44*, 2445 – 2451.

(41) Nguyen, T. X.; Cohaut, N.; Bae, J.-S.; Bhatia, S. K. *Langmuir* **2008**, *24*, 7912–7922.

(42) Senel, A. G.; Guruz, A. G.; Yucel, H.; Kandas, A. W.; Sarofim, A. F. *Energy & Fuels* **2001**, *15*, 331–338.

(43) Kurniawan, Y.; Bhatia, S. K.; Rudolph, V. *AIChE Journal* **2006**, *52*, 957–967.

(44) Subramaniyan, A. K.; Sun, C. *International Journal of Solids and Structures* **2008**, *45*, 4340 – 4346.

(45) Jouanna, P.; Brocas, S. *Comptes Rendus de l'Académie des Sciences - Series IIB - Mechanics* **2001**, *329*, 775 – 782.

(46) Span, R.; Wagner, W. *International Journal of Thermophysics* **2003**, *24*, 41–109.

(47) Harris, J. G.; Yung, K. H. *The Journal of Physical Chemistry* **1995**, *99*, 12021–12024.

(48) Span, R.; Wagner, W. *International Journal of Thermophysics* **2003**, *24*, 111–162.

(49) Vrabec, J.; Stoll, J.; Hasse, H. *The Journal of Physical Chemistry B* **2001**, *105*, 12126–12133.

(50) Zhang, Y.; Yang, J.; Yu, Y.-X. *The Journal of Physical Chemistry B* **2005**, *109*, 13375–13382.

(51) Ozdemir, E.; Morsi, B. I.; Schroeder, K. *Fuel* **2004**, *83*, 1085–1094.

(52) Mirzaeian, M.; Hall, P. J. *Energy & Fuels* **2006**, *20*, 2022–2027.

(53) Gasteiger, J.; Marsili, M. *Tetrahedron* **1980**, *36*, 3219 – 3228.

(54) Israelachvili, J. N. *Intermolecular and Surface Forces, Second Edition: With Applications to Colloidal and Biological Systems (Colloid Science)*; Academic Press, 1992.

(55) Petersen, T.; Yarovsky, I.; Snook, I.; McCulloch, D. G.; Opletal, G. *Carbon* **2004**, *42*, 2457–2469.

(56) Ruthven, D. M. *Principles of adsorption and adsorption processes*; Wiley-Interscience, 1984.

(57) Ettre, L. S. *Pure Appl. Chem.* **1993**, *65*, 819–872.

(58) Ottiger, S.; Pini, R.; Storti, G.; Mazzotti, M.; Bencini, R.; Quattrocchi, F.; Sardu, G.; Deriu, G. *Environ. Prog.* **2006**, *25*, 355–364.

(59) Coussy, O. *Poromechanics*; John Wiley & Sons, Ltd, 2004.

(60) Shuttleworth, R. *Proceedings of the Physical Society. Section A* **1950**, *63*, 444.

(61) Gibbs, J. W. *The collected works*; Longmans (New-York), Green (New-York), 1928; Vol. I.

(62) Haines, R. S.; McIntosh, R. *J. Chem. Phys.* **1947**, *15*, 28–38.

(63) Yakovlev, V.; Fomkin, A.; Tvardovski, A. *Journal of Colloid and Interface Science* **2003**, *268*, 33–36.

(64) Radovic, L. R.; Menon, V. C.; Leon Y Leon, C. A.; Kyotani, T.; Danner, R. P.; Anderson, S.; Hatcher, P. G. *Adsorption* **1997**, *3*, 221–232.

(65) Cui, X.; Bustin, R. M.; Dipple, G. *Fuel* **2004**, *83*, 293–303.

(66) Bae, J.-S.; Bhatia, S. K.; Rudolph, V.; Massarotto, P. *Energy & Fuels* **2009**, *23*, 3319–3327.

(67) Busch, A.; Gensterblum, Y.; Krooss, B. M. *International Journal of Coal Geology* **2003**, *55*, 205–224.